

# Nonlinear dielectric properties of random paraelectric-dielectric composites

Viktor Myroshnychenko<sup>a,\*</sup>, Stanislav Smirnov<sup>a</sup>, Pious Mathews Mulavarickal Jose<sup>a</sup>,  
Christian Brosseau<sup>b</sup>, Jens Förstner<sup>a</sup>

<sup>a</sup>*Institute of Electrical Engineering, Paderborn University, Warburger Straße 100, D-33098 Paderborn, Germany*

<sup>b</sup>*Univ. Brest, CNRS, Lab-STICC, CS 93837, 6 avenue Le Gorgeu, 29238 Brest Cedex 3, France*

---

## Abstract

The challenge of designing new tunable nonlinear dielectric materials with tailored properties has attracted an increasing amount of interest recently. Herein, we study the effective nonlinear dielectric response of a stochastic paraelectric-dielectric composite consisting of equilibrium distributions of circular and partially penetrable disks (or parallel, infinitely long, identical, partially penetrable, circular cylinders) of a dielectric phase randomly dispersed in a continuous matrix of paraelectric phase. The random microstructures were generated using the Metropolis Monte Carlo algorithm. The evaluation of the effective permittivity and tunability were carried out by employing either a Landau thermodynamic model or its Johnson's approximation to describe the field-dependent permittivity of the paraelectric phase and solving continuum-electrostatics equations using finite element calculations. We reveal that the percolation threshold in this composite governs the critical behavior of the effective permittivity and tunability. For microstructures below the percolation threshold, our simulations demonstrate a strong nonlinear behaviour of the field-dependent effective permittivity and very high tunability that increases as a function of dielectric phase concentration. Above the percolation threshold, the effective permittivity shows the tendency to linearization and the tunability dramatically drops down. The highly reduced permittivity and extraordinarily high tunability are obtained for the composites with dielectric impenetrable disks at high concentrations, in which the triggering of the percolation tran-

---

\*Corresponding author

*Email address:* viktor.myroshnychenko@gmail.com (Viktor Myroshnychenko)

sition is avoided. The reported results cast light on distinct nonlinear behaviour of 2D and 3D stochastic composites and can guide the design of novel composites with the controlled morphology and tailored permittivity and tunability.

*Keywords:* Paraelectric-dielectric composite, Tunability, Effective permittivity, Landau-Devonshire theory, Percolation, Nonlinear dielectric properties

---

## 1. Introduction

Ferroelectric materials have attracted significant scientific and practical attention in last decades due to their highly nonlinear dielectric response to an applied electric field in microwaves range [1, 2]. In particular, ferroelectrics in a paraelectric state are characterized by the absence of polarization hysteresis, relatively low dielectric losses and leakage currents, high dielectric permittivity which nonlinearly depends on the applied electric field, and high tunability at microwave frequency. These peculiar properties of paraelectrics find potential application in microelectronic circuits and voltage tunable microwave devices, such as tunable mixers, varactors, oscillators, phase shifters, capacitors, delay lines, and filters [3–7]. Ferroelectrics such as (Ba,Sr)TiO<sub>3</sub>, Ba(Zr,Ti)O<sub>3</sub>, and (Pb,Sr)TiO<sub>3</sub> have been demonstrated to be potential candidates for such applications [8–10]. However, the high dielectric tunability in single-phase ferroelectrics is usually accompanied by large permittivity ( $\sim 1000$ ) that might be undesirable for some applications which simultaneously require to maintain high tunability and reduced permittivity while keeping low losses [4, 11]. To address this major challenge in designing materials for tunable devices, several methods were proposed, e.g., doping ferroelectrics with different ions [12] and fabrication of a variety of composite mixtures of a nonlinear paraelectric and a linear low-loss dielectric (oxides, polymers, and pores) phases [13–17]. It has been demonstrated that specially designed ferroelectric composite structures possess even improved tunability than those of single phase nanonlinear materials due to the interfacial phenomena between distinct phases and the resulting local electric field inhomogeneity and enhancement. Actually, it has been known for many years that the functional properties of composites are strongly dependent on their microstructures [18]. Therefore, the ability to control and manipulate microstructures of a composite offers a practical way to tailor both permittivity and tunability to desired values [19, 20].

25 The determination of the effective dielectric response of composite materials has been  
the subject of continuous attention over several decades [21–23]. With regard to linear  
macroscopic electromagnetic response of these materials, physicists engaged in this area  
have developed approximate analytical effective-medium theories (EMT) and other mean-  
field-like approximations to describe their behaviour [24, 25]. However, many of these theories  
30 can be applied only to a specific combination of particles-host medium taking into account  
simple microstructure information such as volume fraction and inclusion shape, furthermore,  
they are based on dipolar interactions only. A number of authors have developed modified  
EMTs for nonlinear ferroelectric-dielectric composites, by coupling EMTs with the expression  
for field-dependent permittivity of the ferroelectric material described by phenomenological  
35 Landau-Devonshire (LD) theory [26, 27]. However, due to the complexity of the multipolar  
interactions between inclusions and an environment and, in turn, the intense local electric  
field fluctuations, modified EMTs cannot be predictive for general situations.

Therefore, a number of recent works have considered a numerical approach to this problem  
within the long wavelength limit [28–31]. These investigations focus on modeling the effective  
40 nonlinear permittivity and tunability of several ferroelectric-dielectric systems by integrating  
the field-dependent permittivity of a ferroelectric, described by either LD theory or Johnson’s  
equation (JE), into a finite element analysis. In particular, it has been shown that the porous  
(Ba,Sr)TiO<sub>3</sub>- and Pb(Zr,Ti)O<sub>3</sub>-based ceramics exhibit a higher tunability and significantly  
reduced permittivity comparable to those of the bulk ceramics [32–34]. However, further  
45 efforts are still needed to fully understand the numerically and experimentally observed  
features of the nonlinear behaviour of ferroelectric composites. For examples, there is a  
need for systematic investigation of (i) how the randomness and connectedness influence  
the effective permittivity and tunability, (ii) how dielectric response of percolative systems  
change near and above the percolation threshold, (iii) how interactions between aggregates  
50 and agglomerates, which are always formed within a host matrix, affect interfacial and  
multipolar interactions. All of these structural features give rise to extremely rich physics  
not fully explored so far.

In this paper, we report on a comprehensive numerical study of effective nonlinear di-  
electric properties of a 2D random paraelectric-dielectric composite in the long-wavelength

55 limit. The composite is composed of identical circular disks, with an arbitrary degree of  
 impenetrability, made of a linear lossless dielectric randomly distributed throughout a con-  
 tinuous paraelectric host matrix. The 3D analog of this model would be a composite consist-  
 ing of parallel infinitely long, identical, partially penetrable cylinders randomly distributed  
 throughout a host matrix, where the properties and characteristics are invariant along the  
 60 cylinder axis. The generation of random microstructures was carried out using the standard  
 Metropolis Monte Carlo algorithm. The permittivity field dependence of the paraelectric  
 phase are specified through a nonlinear thermodynamic model using either the LD theory  
 of phase transformations or its Johnson’s approximation and then built-in into a finite ele-  
 ment method (FEM) analysis, which solves continuum-electrostatics equations for the local  
 65 potential. We demonstrate the great potential of this combined numerical technique by ac-  
 cessing spatially resolved electric fields in composites and computing field-dependent effective  
 permittivity and tunability over wide ranges of various parameters, including the intrinsic  
 constituent permittivity, the surface fraction, and the degree of disk impenetrability. Our  
 simulations reveal a strong nonlinear behaviour of the effective permittivity and extraordi-  
 70 narily high tunability. Furthermore, we show that the randomness and connectedness of the  
 particle phase can dramatically influence the tunability of the paraelectric-dielectric compos-  
 ite and reveal its critical dependence on the percolation threshold. Finally, our comparative  
 study of results obtained by using the LD theory and its Johnson’s approximation for the  
 description of permittivity in a paraelectric phase unveils unexpected underlying differences  
 75 in the nonlinear response and tunability of the composite.

## 2. Dielectric nonlinearity of paraelectrics

### 2.1. Landau-Devonshire theory

Here, we focus on ferroelectrics in the paraelectric state as dielectrically isotropic mate-  
 rials whose dielectric permittivity changes significantly under the applied external electric  
 field. This dielectric nonlinearity can be phenomenologically treated within the framework  
 of LD theory, where the Gibbs free energy of a ferroelectric cubic crystal free of stress/strain  
 and space charges is described in terms of macroscopic polarization as [35, 36]

$$F(P, T, E) = \frac{\alpha}{2}P^2 + \frac{\beta}{4}P^4 + \frac{\gamma}{6}P^6 + \dots, \quad (1)$$

where  $T$ ,  $E$ , and  $P$  are the temperature, applied electric field, and equilibrium polarization at a given field, respectively, and  $\alpha$ ,  $\beta$ ,  $\gamma$  are Landau coefficients. The coefficient  $\alpha = C(T - T_0) = 1/(\varepsilon_0\varepsilon_r(0))$  given by the Curie-Wiess law is temperature-dependent, where  $C$  is the Curie-Wiess constant,  $T_0$  is the Curie-Wiess temperature,  $\varepsilon_r(0)$  is the relative dielectric permittivity at zero dc electric field (positive in paraelectric state), and  $\varepsilon_0$  is the permittivity of free space. The coefficients of the ferroelectric nonlinearity  $\beta$  and  $\gamma$  are generally smooth functions of temperature. When a dc electric field is applied to the paraelectric phase and assuming  $\gamma = 0$ , the energy of the system can be written as

$$F(P, T, E) = \frac{\alpha}{2}P^2 + \frac{\beta}{4}P^4 - P \cdot E. \quad (2)$$

Stable states of the system are characterized by minima of the free energy, i.e.,  $\partial F(P, T, E)/\partial P = 0$ , leading to

$$E = \alpha P + \beta P^3. \quad (3)$$

In a nonzero bias field, the relative dielectric permittivity of the system parallel to the applied electric field is defined as

$$\varepsilon_r(E) = \left[ \varepsilon_0 \frac{\partial^2 F(P, T, E)}{\partial P^2} \right]^{-1}, \quad (4)$$

where the derivative  $\partial^2 F/\partial P^2$  is derived from Eq. 2. Finally, the dependence of the relative permittivity on the applied electric field in accordance to the LD theory is described by the equation

$$\varepsilon_r(E) = \frac{1}{\varepsilon_0(\alpha + 3\beta P^2)}, \quad (5)$$

where the electric field induced polarization  $P(E)$  is obtained by solving Eq. 3. It is worth noting that this approach well describes paraelectrics close and above the Curie temperature under the assumptions of homogeneity of the electric field within the material, negligible contributions of stress/strain to the total energy, and in the absence of charges. This theory will be used for the local description of the paraelectric material inside the composite and integrated in our FEM analysis, denoted as LD-FEM and described in the next section.

## 2.2. Johnson's equation

Note that the Eq. 5 implicitly includes the electric field dependence of the dielectric permittivity leading to a more complicated implementation. To overcome this issue, Johnson

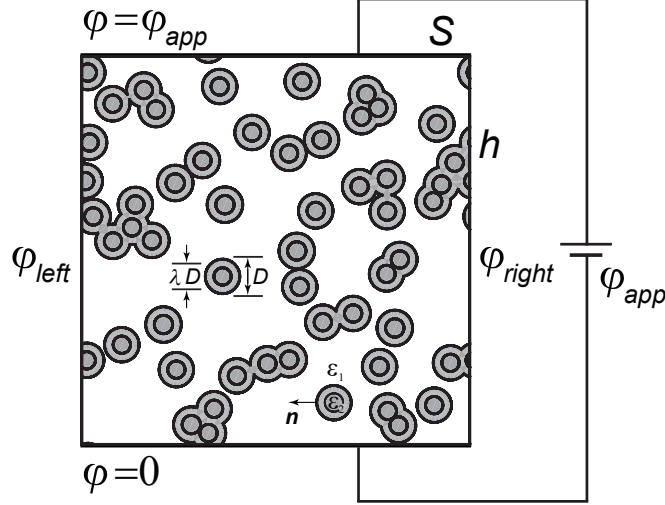


Figure 1: Illustration of the calculation of the field-dependent effective permittivity with boundary conditions for a typical sample realization of the two-phase composite consisting of monodisperse circular disks, of linear dielectric permittivity  $\varepsilon_2$ , surface fraction  $\phi_2$  and with a degree of impenetrability  $\lambda(0 \leq \lambda \leq 1)$ , randomly dispersed within the nonlinear paraelectric host material of permittivity  $\varepsilon_1$  and surface fraction  $\phi_1 = 1 - \phi_2$ . Each disk of diameter  $D$  is composed of a mutually impenetrable core of diameter  $\lambda D$  (region inside inner black circle) encompassed by a perfectly penetrable shell of thickness  $(1 - \lambda)D/2$ . The application of periodic boundary conditions leads to the structure spanning the whole 2D space.

derived an explicit approximative solution for describing the field-dependent dielectric constant of paraelectrics from the LD theory, assuming small polarization values approximated as  $P(E) = \varepsilon_0 \varepsilon_r(E) E$  [37]

$$\varepsilon_r(E) = \frac{\varepsilon_r(0)}{(1 + 3\beta(\varepsilon_r(0)\varepsilon_0)^3 E^2)^{1/3}}. \quad (6)$$

85 This equation has been tested successfully with experimental results for some paraelectric materials up to high dc electric field [13–17, 38, 39]. The Johnson’s equation (JE) was also built in our FEM simulations, denoted as JE-FEM, and its applicability was studied by comparison with the LD-FEM results. Besides, the JE was also used to fit numerical results calculated by using LD-FEM and determine the effective Landau coefficient of the dielectric  
 90 nonlinearity  $\beta_{eff}$  of the considered composite systems.

### 3. Methodology and numerical implementation

We consider a two-phase composite medium consisting of monodisperse circular disks with an arbitrary degree of impenetrability  $\lambda(0 \leq \lambda \leq 1)$  of linear dielectric material with permittivity  $\varepsilon_2$  and area fraction  $\phi_2$  randomly placed in the host of nonlinear paraelectric material with field-dependent permittivity  $\varepsilon_1(E)$  and area fraction  $\phi_1 = 1 - \phi_2$ . The disks are allowed to overlap with each other with an arbitrary degree of impenetrability  $\lambda(0 \leq \lambda \leq 1)$ , i.e., each disk of diameter  $D$  is composed of an impenetrable core of diameter  $\lambda D$ , which is encompassed by a penetrable concentric shell of thickness  $(1 - \lambda)D/2$ . The extreme limits  $\lambda = 0$  and  $\lambda = 1$  correspond to fully penetrable disks and the totally impenetrable disks, respectively. Thus, by continuously varying  $\lambda$  between 0 and 1, one can vary the exclusion-area effects and, hence, the connectedness of the inclusions. The surface fraction occupied by the disks,  $\phi_2$ , varies between 0 and the maximum packing fraction. The representative realization of such two-phase composite is illustrated in Figure 1. Note that the inclusions investigated can be considered as circular cross sections of infinite 3D parallel partially-penetrable cylinders, where the properties and characteristics are invariant along the cylinder axis.

Below, we provide a brief description of the procedures for (a) generation of realizations of the random two-phase medium using the statistically based standard Metropolis Monte Carlo algorithm and (b) numerical evaluation of the field-dependent effective permittivity and tunability of the paraelectric-dielectric composite using the FEM combined with either the LD or Johnson's equations.

#### 3.1. Generation of random two-phase microstructures

We used the traditional Metropolis Monte Carlo (MC) algorithm in 2D to generate the random two-phase microstructures of equilibrium distributions of disks at a specified disk surface fraction  $\phi_2$  and degree of impenetrability  $\lambda$  [40, 41]. The explanation and details of the key steps of this algorithm, producing statistically homogeneous and isotropic equilibrated realizations of the composite, can be found in Refs. [42–44]. Periodic boundary conditions were employed in order to minimize boundary effects due to the finite size of the system, i.e., the unit cell containing the particles is repeated periodically within the plane to form

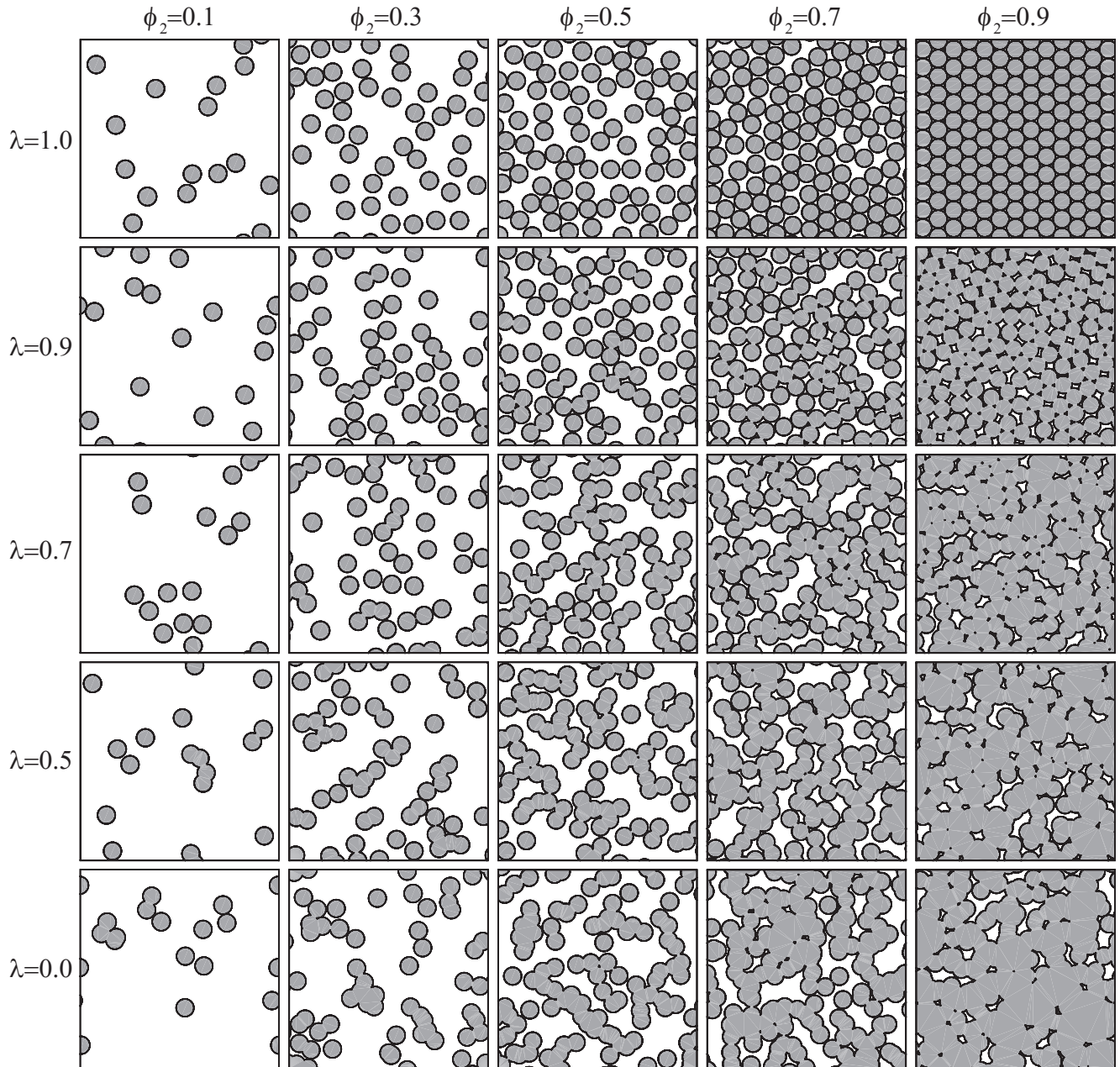


Figure 2: Typical equilibrium sample realizations illustrating the local microstructure of the two-phase composite consisting of monodisperse circular partially penetrable disks randomly distributed within a square matrix. The sample packing results from the sequential algorithm described in the text applied to a binary mixture at a specified disk surface fraction  $\phi_2 (0 \leq \phi_2 \leq 1)$  and degree of impenetrability  $\lambda (0 \leq \lambda \leq 1)$ .

120 an infinite lattice. Figure 2 shows typical random configurations of medium for selected values of  $\lambda$  and  $\phi_2$  demonstrating the qualitative differences of these images related to the dramatic clustering behavior as  $\lambda$  and  $\phi_2$  are varied. Once the equilibrium realization of the composite medium are generated then the FEM analysis for finding the field-dependent effective permittivity and tunability is started, as discussed in the next subsection.

### 125 3.2. Model of the effective permittivity of paraelectric-dielectric media

The LD (Eq. 5) and Johnson’s (Eq. 6) equations presented in section 2 describe nonlinear dielectric permittivity of single phase paraelectrics, however, they fail to characterise highly disordered and inhomogeneous microstructures which generate strong spatial electric field fluctuations under an applied field. Therefore, in this work, we combine the LD and Johnson’s equations for the local description of dielectric permittivity of a paraelectric phase with a  
 130 2D FEM analysis to accurately evaluate the local field inhomogeneity in composites. In what follow, we present a method suitable for determining nonlinear dielectric properties of paraelectric-dielectric heterostructures in the quasistatic limit.

We consider a parallel plate capacitor, with conducting plates of area  $S$  and separation distance between electrodes  $h$ , which is filled with the di-phase composite under consideration as shown in Figure 1 [45]. The medium consists of an isotropic paraelectric material with the space- and field-dependent relative permittivity  $\varepsilon_1$  (matrix phase 1) and a dielectric material with constant relative permittivity  $\varepsilon_2$  (disks phase 2). A potential difference  $\varphi_{app}$  is applied between the capacitor plates. Assuming that  $h$  is small enough, i.e., fringing effects can be ignored, the “macroscopic” field-dependent effective permittivity  $\varepsilon_{eff}(E_{app})$  can be determined from the electrostatic energy  $W$  stored in the capacitor as

$$W = \frac{1}{2} \varepsilon_0 \varepsilon_{eff}(E_{app}) \frac{S}{h} \varphi_{app}^2, \quad (7)$$

where  $E_{app} = \varphi_{app}/h$  is the applied external field. This definition ensures us that the energy stored in the capacitor would be the same if the composite medium was replaced by a homogeneous medium with permittivity  $\varepsilon_{eff}(E_{app})$  subject to the same boundary conditions. Alternatively, the energy  $W$  can be expressed in terms of the spatial distribution of the electrostatic potential  $\varphi(\mathbf{r})$  inside the capacitor if the microscopic structure of the material

is known. Since the composite considered here is locally isotropic, the energy  $W$  over the surface  $\Omega$  of the capacitor is

$$W = \frac{1}{2}\varepsilon_0 \int_{\Omega} \varepsilon(\mathbf{r})[\nabla\varphi(\mathbf{r})]^2 d^2\mathbf{r}, \quad (8)$$

where  $\varepsilon(\mathbf{r})$  is the local relative permittivity at the position  $\mathbf{r}$ . Thus, determining the effective permittivity of the composite medium requires knowledge of the distribution of the local electrostatic potential  $\varphi(\mathbf{r})$ . This can be done by solving the boundary value problem described by the Laplace's equation

$$\nabla \cdot [\varepsilon(\mathbf{r})\nabla\varphi(\mathbf{r})] = 0 \quad (9)$$

in conjunction with the boundary conditions  $\varphi_{bottom} = 0$  at the bottom plate and  $\varphi_{top} = \varphi_{app}$  at the top plate. Edge fringing effects can be eliminated by the periodic extension of the capacitor. For that purpose, we apply periodic boundary conditions on the left and right boundaries of the unit cell, i.e.,  $\varphi_{left} = \varphi_{right}$ . The local permittivity of the dielectric disks  $\varepsilon_2(\mathbf{r})$  is field-independent and homogeneous inside the phase. Contrarily, the relative permittivity of the paraelectric matrix  $\varepsilon_1(E(\mathbf{r}))$  depends on the local electric field acting at the corresponding position  $\mathbf{r}$  and, thus, can be highly inhomogeneous inside the phase. It is locally evaluated by using either the LD or Johnson's equations as

$$\varepsilon_1(E(\mathbf{r})) = \frac{1}{\varepsilon_0(\alpha + 3\beta P^2(\mathbf{r}))} \quad (10)$$

and

$$\varepsilon_1(E(\mathbf{r})) = \frac{\varepsilon_1(0)}{(1 + 3\beta(\varepsilon_1(0)\varepsilon_0)^3 E^2(\mathbf{r}))^{1/3}}, \quad (11)$$

respectively, where  $E(\mathbf{r}) = -\nabla\varphi(\mathbf{r})$  is the local electric field at the position  $\mathbf{r}$  and  $P(\mathbf{r})$  is the field induced local polarization obtained by solving Eq. 3 locally, i.e.,  $E(\mathbf{r}) = \alpha P(\mathbf{r}) + \beta P^3(\mathbf{r})$ . In this case, both  $E(\mathbf{r})$  and  $P(\mathbf{r})$  are the projections of the corresponding local fields on the applied field direction.

Due to the nonlinear nature of the paraelectric phase material, the field-dependent effective permittivity  $\varepsilon_{eff}(E_{app})$  was obtained using the iterative procedure by successively solving the Laplace's Eq. 9 in a range of the applied voltages from 0 V to  $\varphi_{max}$  with a small step, similar to the one proposed by Padurariu et al. [30]. At each voltage step, the local

permittivities in the paraelectric phase only are recomputed employing either LD Eq. 10 or Johnson’s Eq. 11 by using the local polarizations  $P(\mathbf{r})$  or local electric fields  $E(\mathbf{r})$ , respectively, calculated at the previous voltage step. This means that the local permittivity will be scattered in values in the paraelectric phase depending on the degree of local field inhomogeneity. Once Eq. 9 is solved for the local potential, the energy stored in the capacitor is calculated using Eq. 8 and, finally, field-dependent effective permittivity  $\varepsilon_{eff}(E_{app})$  is obtained from Eq. 7. To characterize the dielectric nonlinearity of composites, we will use the absolute tunability parameter defined as the ratio

$$n(E_{app}) = \frac{\varepsilon_{eff}(0)}{\varepsilon_{eff}(E_{app})}, \quad (12)$$

where  $\varepsilon_{eff}(0)$  is the effective permittivity at zero field and  $\varepsilon_{eff}(E_{app})$  is that in the presence of the external field  $E_{app}$ .

### 140 3.3. Summary and further computational details

To summarize, our procedure for the calculation of field-dependent effective properties of the random paraelectric-dielectric composite outlined in the previous subsections is as follows. First, generate randomly distributed disk configurations in a square box for a specified disk surface fraction  $\phi_2$  and degree of impenetrability  $\lambda$  using the MC algorithm. In all calculations a square unit cell of size  $L = 1$  cm and the disks’ diameter  $D = 0.09$  cm were  
145 maintained constant. Depending on the value of surface fraction of disks  $\phi_2$ , impenetrability parameter  $\lambda$  and statistical distribution of the disks in the system, the generated realizations consist of from 16 to about 450 disks in the unit cell. Previous simulations have indicated that such number of inclusions is acceptable for our purpose [45]. Second, carry out the  
150 calculation of the field-dependent effective permittivity ( $\varepsilon_{eff}(E_{app})$ ) and tunability ( $n(E_{app})$ ) for each generated realization of medium by separately employing the LD-FEM and JE-FEM models. They are calculated at different values of the applied external field in the range from 0 kV/cm to 30 kV/cm generated by a potential difference  $\varphi_{app}$  across the vertical edges of the computational unit cell with the same boundary conditions. The majority of  
155 our simulation results pertain to the following set of parameters: the relative permittivity of the linear disk phase  $\varepsilon_2 = 1$ , i.e. we consider a porous paraelectric material; for the nonlinear matrix phase the zero-field relative permittivity  $\varepsilon_1(0) = 1000$ , which is typical

for the prototype Pb(Zr,Ti)O<sub>3</sub>-based ferroelectric, Landau coefficients  $\alpha = 1/(\varepsilon_0\varepsilon_1(0)) = 1.129 \cdot 10^8 \text{ V}\cdot\text{m}/\text{C}$ , and  $\beta = 4.821 \cdot 10^{11} \text{ V}\cdot\text{m}^5/\text{C}^3$ , unless otherwise stated [33, 46]. Finally, the effective permittivity and tunability are evaluated by averaging over the results for 200 statistically independent realizations of the random system at specified  $\phi_2$  and  $\lambda$ . Note that the statistical averaging over 400 realizations is performed for the disk surface fractions in the range  $0.6 \leq \phi_2 \leq 0.8$  due to large variance in the values of  $\varepsilon_{eff}$ . The surface fraction occupied by the linear dielectric disks varies in this study between 0 and 0.9. Because our numerical results for the field-dependent effective permittivity and tunability do not show a significant sensitivity to the degree of impenetrability  $\lambda$  of the disks in the range between 0 and 0.5, we present our results only for the discrete values of  $\lambda = 0, 0.7, 0.9, 1$ . We used the FEM-based COMSOL Multiphysics<sup>®</sup> software [47] with the aid of Java environment to perform the generation of random composites and calculation of the effective parameters.

#### 4. Results and discussion

It should be stressed from the very start that we actually deal with two models of 2D random heterostructures here. In the first model, we consider nonpercolating systems consisting of nonoverlapping hard disks ( $\lambda = 1$ ) for which there is always a minimum allowable separation distance between disks, and thus, particle–particle contacts are avoided. In the second model, disks are allowed to overlap with each other to some degree ( $0 \leq \lambda < 1$ ) and possess the geometrical percolation threshold at the critical surface fraction  $\phi_{2c}$ , i.e., the point at which particles (a disconnected phase) form the so-called infinite cluster or pathways spanning the composite. In continuum-percolating systems, the percolation threshold depends on the shape and orientation of the particles and on correlations between the spatial positions of their centers. In our 2D systems, the thresholds are reported to be  $\phi_{2c} = 0.69, 0.71, 0.76, 0.84$  for the impenetrability parameter  $\lambda = 0, 0.7, 0.9, 1$ , respectively [43].

We start our study of macroscopic response of different configurations of the composite computed by using the LD-FEM model. The field-dependent effective permittivity and tunability as a function of applied field at selected values of the disk area fraction  $\phi_2$  and degree of impenetrability  $\lambda$  are presented in Figure 3. A drastically different behaviour is observed depending on whether the disks are allowed to penetrate or not and whether the

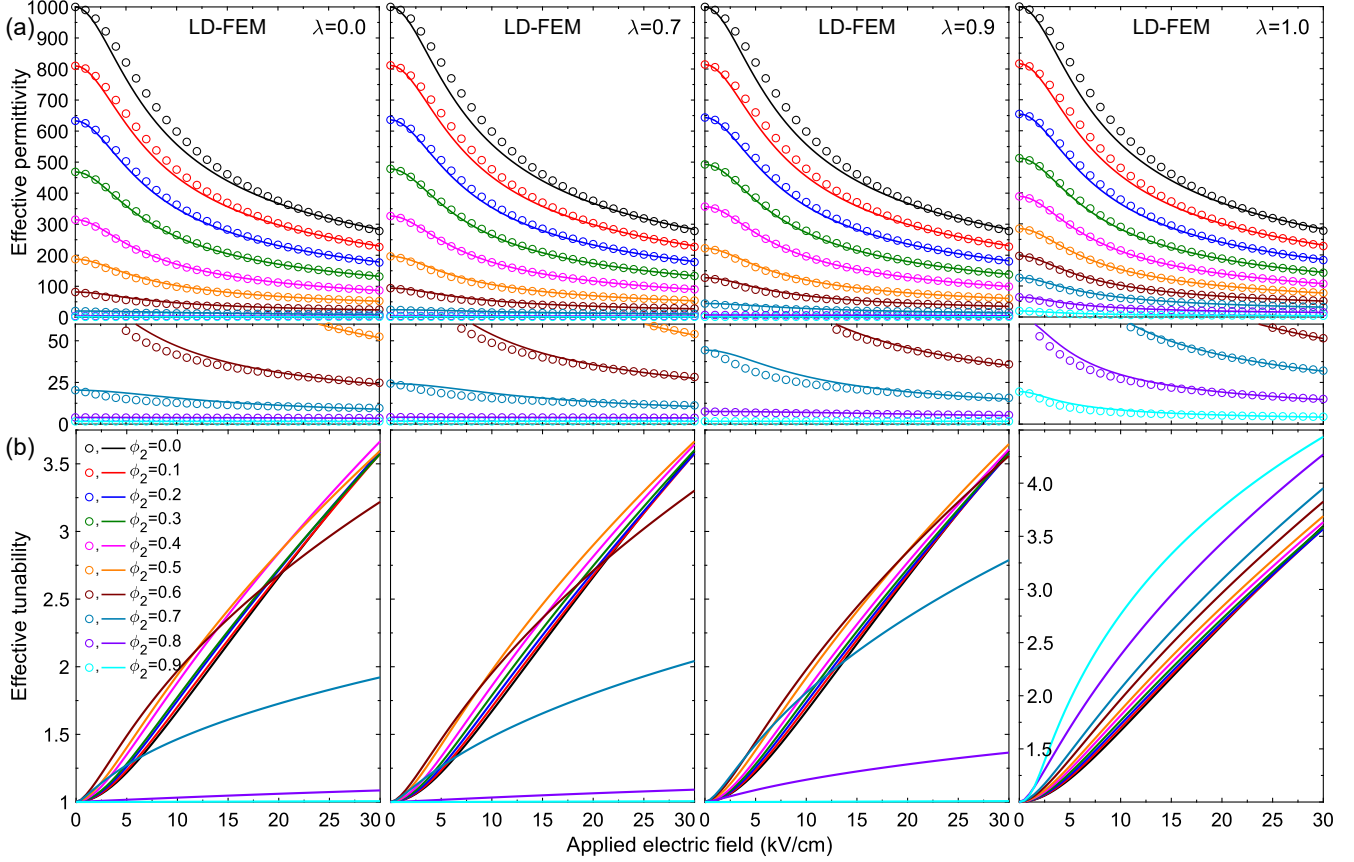


Figure 3: Effective permittivity (a, dots) and tunability (b, curves) of the random composite as a function of the applied electric field calculated by using LD-FEM model for different values of the linear dielectric phase (disks) surface fraction  $\phi_2$  from 0 to 0.9 and degree of impenetrability  $\lambda = 0, 0.7, 0.9, 1$ . Continuous curves in (a) correspond to fitting the calculated field-dependent effective permittivity (dots) with Johnson's Eq. 6 using the determined effective Landau coefficient  $\beta_{eff}$  shown in Figure 6(a).

system is below, near, or above the percolation threshold.

For the structures with penetrable disks ( $0 \leq \lambda \leq 0.9$ ), the data shows a highly nonlinear behaviour of effective permittivity as a function of applied field accompanied by a monotonic reduction of zero-field permittivity (Figure 3(a), dots) and an increase of tunability (Figure 3(b), curves) with increasing the surface fraction of disks up to the value well below the percolation threshold for a particular  $\lambda$ . The decrease of the zero-field permittivity is primarily due to the reduction of surface fraction of the high permittivity paraelectric phase and, consequently, a decrease of the electrical energy stored in the composite. This is

195 counterbalanced by the induced local electric field inhomogeneity inside the composite which  
 increases as  $\phi_2$  increases, resulting in an effect of preserving the strong  $\varepsilon_{eff}(E_{app})$  variation  
 and thus even higher tunability than for the bulk paraelectric phase. This is illustrated  
 in Figure 4, showing the calculated local electric field maps in the unit cell at the applied  
 electric field  $E_{app} = 1 \text{ kV/cm}$  for typical configurations at a specified disk surface fraction  $\phi_2$   
 200 and degree of impenetrability  $\lambda$ . As can be seen, the degree of electric field inhomogeneity  
 strongly and monotonically increases with increasing the number of disks (pores) in the cell.  
 Interestingly, the highly inhomogeneous field is observed inside the disks and outside the  
 disks in close vicinity to the matrix-disk boundaries. These plots also reveal the presence of  
 regions of high field intensity when particles are in close contact with each other arising from  
 205 the short-range multipolar interactions localized in disk clusters. Furthermore, we observe a  
 high degree of long-range interparticle coupling when disk contacts form partially connected  
 or disconnected finite chain spanning the cell in a direction approximately perpendicular to  
 the applied field. This coupling leads to a significant potential-bridging involving a huge field  
 intensity enhancements (hot spots) along the chain confined inside the disks and in the gap  
 210 areas between the disks in the paraelectric phase (e.g. see a plot for  $\lambda = 0.9$  and  $\phi_2 = 0.3$   
 in Figure 4) and, in turn, strongly influences the effective permittivity. As the number of  
 disks in the cell increases (i.e.  $\phi_2$  increases) and the disk-disk distances diminish, the prob-  
 ability of finding regions of high field intensity rises significantly. Because the permittivity  
 of paraelectrics strongly depends on the applied electric field (see Eq. 10), these regions of  
 215 high field intensity greatly modify the local permittivities in such a way it compensates for  
 the reduction of paraelectric phase in the composite and produces enough non-linearity for  
 the same or even higher tunability as in the bulk paraelectric.

We now continue considering the structures with penetrable disks but with disk surface  
 fractions near and above the percolation threshold, i.e  $\phi_2 \gtrsim 0.6$ . In this case Figure 3(a)  
 220 indicates that the effective permittivity for all  $\lambda$  exhibits a tendency to a further decrease but  
 with linearization as a function of the applied electric field, while the tunability (Figure 3(b))  
 falls sharply with a different degree depending on  $\lambda$ . Specifically, the effective permittivity is  
 almost field-insensitive for disk surface fractions  $\phi_2 \geq 0.8$  and, thus, the tunability approaches  
 1. It should be noted at this point that the strong decrease of tunability for the concentration

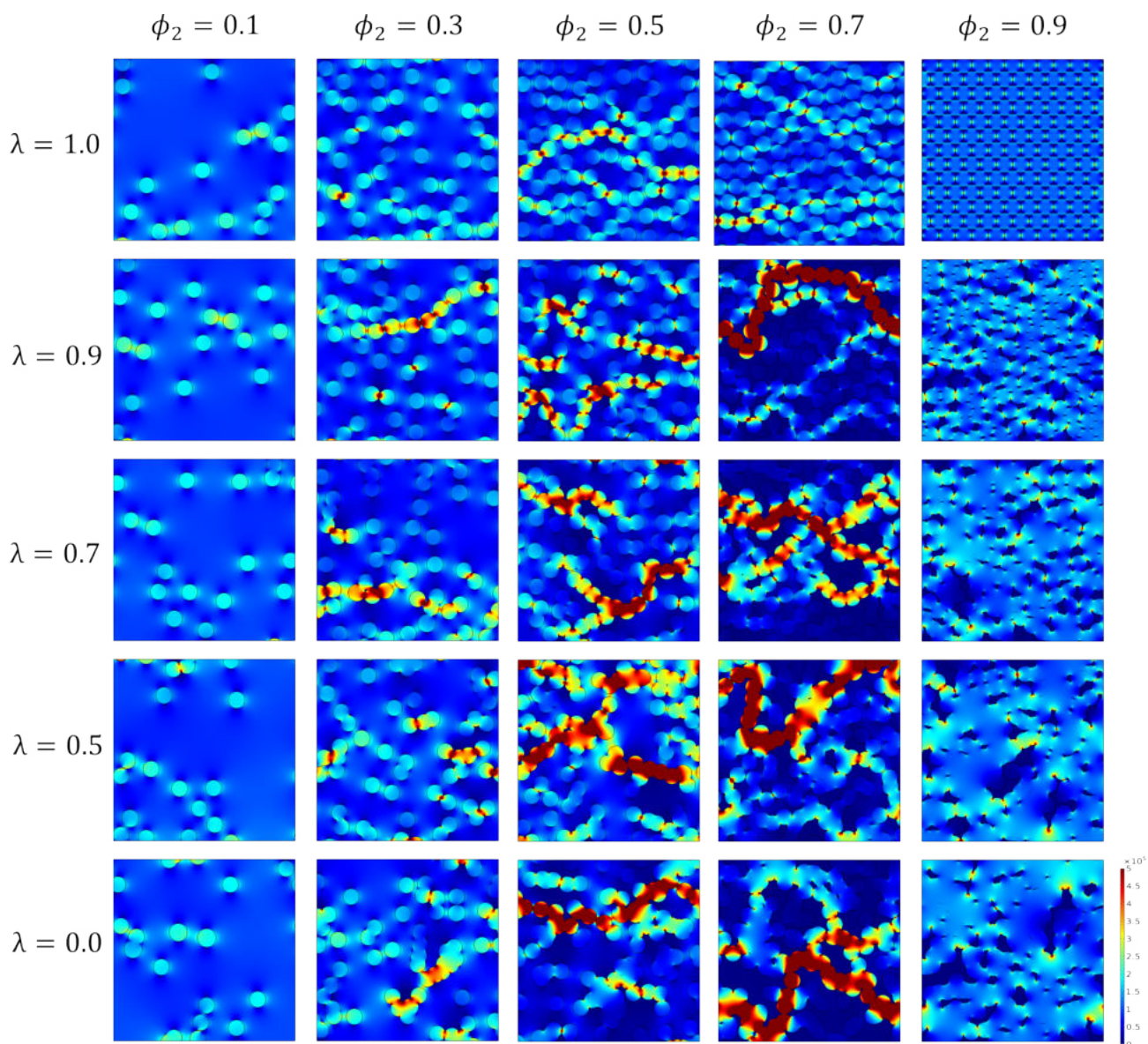


Figure 4: Calculated local electric field maps in the unit cell at the applied electric field  $E_{app} = 1 \text{ kV/cm}$  for typical equilibrium sample configurations at a specified disk surface fraction  $\phi_2 (0 \leq \phi_2 \leq 1)$  and the degree of impenetrability  $\lambda (0 \leq \lambda \leq 1)$ . The side bar gives the values of the electric field corresponding to the colors.

225 of linear dielectric phase above 40% – 50% in other 2D systems has been reported in recent  
 numerical and experimental works, while this behaviour has not been well understood [31,  
 33]. Actually, the abrupt variation of the tunability for the data in the vicinity to the critical  
 surface fraction  $\phi_{2c}$  is a clear indication of the critical transition in the composite associated  
 with the formation of a physically infinite connected cluster of linear dielectric disks spanning  
 230 the cell from the left to right sides, as nicely illustrated in Figure 4 for  $\lambda = 0.9$  and  $\phi_2 = 0.7$ .  
 It is intriguing to observe in this map that when the inclusion phase is sample-spanning  
 in a direction perpendicular to the applied electric field, the paraelectric matrix becomes  
 completely discontinuous. This results in an enormous field intensity concentrated in the  
 low-permittivity dielectric phase along a trajectory of the chainlike structure avoiding high-  
 235 permittivity regions of the nonlinear paraelectric phase. Moreover, the electric field in major  
 regions of the paraelectric phase becomes even weaker than the applied external field that  
 together with its concentration reduction causes a dramatic decrease of the overall effective  
 tunability of the composite.

The situation is completely different for the composite configurations with totally impen-  
 240 etrable disks ( $\lambda = 1$ ). In this case we observe a continuous decrease in nonlinear effective  
 permittivity and an increase in tunability up to the highest disk surface fraction ( $\phi_2 = 0.9$ ).  
 One natural explanation for this behavior is that the structures with forbidden particle-  
 particle overlaps do not possess the geometrical percolation threshold and, thus, the para-  
 electric matrix phase is always continuous, as can be seen in the upper panel of Figure 4. On  
 245 the other hand, in the dense disk configurations, many inclusions approach close contacts  
 that initiates higher order interparticle multipole interactions contributing to the polariza-  
 tion of the paraelectric medium and, thus, produces greatly enhanced electric field confined  
 in the vicinity of small regions between neighboring inclusions. Indeed, the map for  $\lambda = 1$   
 and  $\phi_2 = 0.7$  of Figure 4 clearly shows that the large portion of the remaining paraelectric  
 250 matrix is subjected to the high electric field that is enough to generate a strong nonlinearity  
 in the composite. Therefore, the presence or absence of the geometrical percolation thresh-  
 old in this composite dramatically influences the behavior of the effective permittivity and  
 tunability at mid-high disk surface fractions.

It is also important to emphasize that for a given value of disk surface fraction, the

255 effective permittivity increases as the impenetrability parameter  $\lambda$  is increased (i.e. the  
 degree of disks overlap is decreased), while the tunability does not varies significantly for all  
 random systems below the percolation threshold. This remarkable difference in permittivity  
 is more pronounce for the larger disk volume fractions. It is attributed mainly to the manner  
 in which particles form aggregates and agglomerates in the composite governed by  $\lambda$ , where  
 260 increased aggregation for the smaller  $\lambda$  results in a decreased number of disk-disk and cluster-  
 cluster multipolar interactions and consequently the decreased permittivity. Thus, different  
 combinations of tunability and reduced permittivity can be tailored by manipulating not only  
 the disk surface fraction but also the impenetrability parameter of inclusions in paraelectric  
 composites.

265 We now investigate the behavior of the effective permittivity and tunability of the com-  
 posite by using the JE-FEM model and compare it with the LD-FEM description. Before  
 exploring this model in more detail, it is worth to keep in mind the following difference  
 between Johnson's (Eq. 6) and LD (Eq. 5) equations for the field-dependent permittivity of  
 paraelectrics. The Johnson's approximation is restricted to the linear relationship between  
 270 polarization and external electric field, while the LD description is based on the Gibbs free  
 energy expansion up to the forth order in the polarization which accounts properly for the  
 non-linear behavior of the system. A few comments about the distinction between the sim-  
 ulation results obtained using the JE-FEM (Figure 5) and LD-FEM (Figure 3) models are  
 in order. First of all, the JE-FEM data reveals the same general trend as the LD-FEM data  
 275 for both field-dependent effective permittivity (dots) and tunability (curves). However, the  
 JE-FEM permittivity for all configurations exhibits much weaker nonlinearity, i.e. weaker  
 variation of the effective permittivity versus applied electric field ( $d\varepsilon_{eff}(E_{app})/dE_{app}$ ), and  
 thus much lower tunability. For comparison, the JE-FEM and LD-FEM zero-field effec-  
 tive permittivities for the pure paraelectric ( $\phi_2 = 0$ ) decrease approximately 2.16 and 3.60  
 280 times, respectively, comparing with their corresponding values at 30 kV/cm. Note that the  
 zero-field permittivity in both models monotonically decreases with no tendency towards  
 saturation up to the maximum tested field of 30 kV/cm for all disk surface fractions below  
 percolation thresholds. The second important feature is that the JE-FEM tunability for all  
 percolating systems with  $\phi_2 \lesssim \phi_{2c}$  increases as disk surface fraction is increased at low to

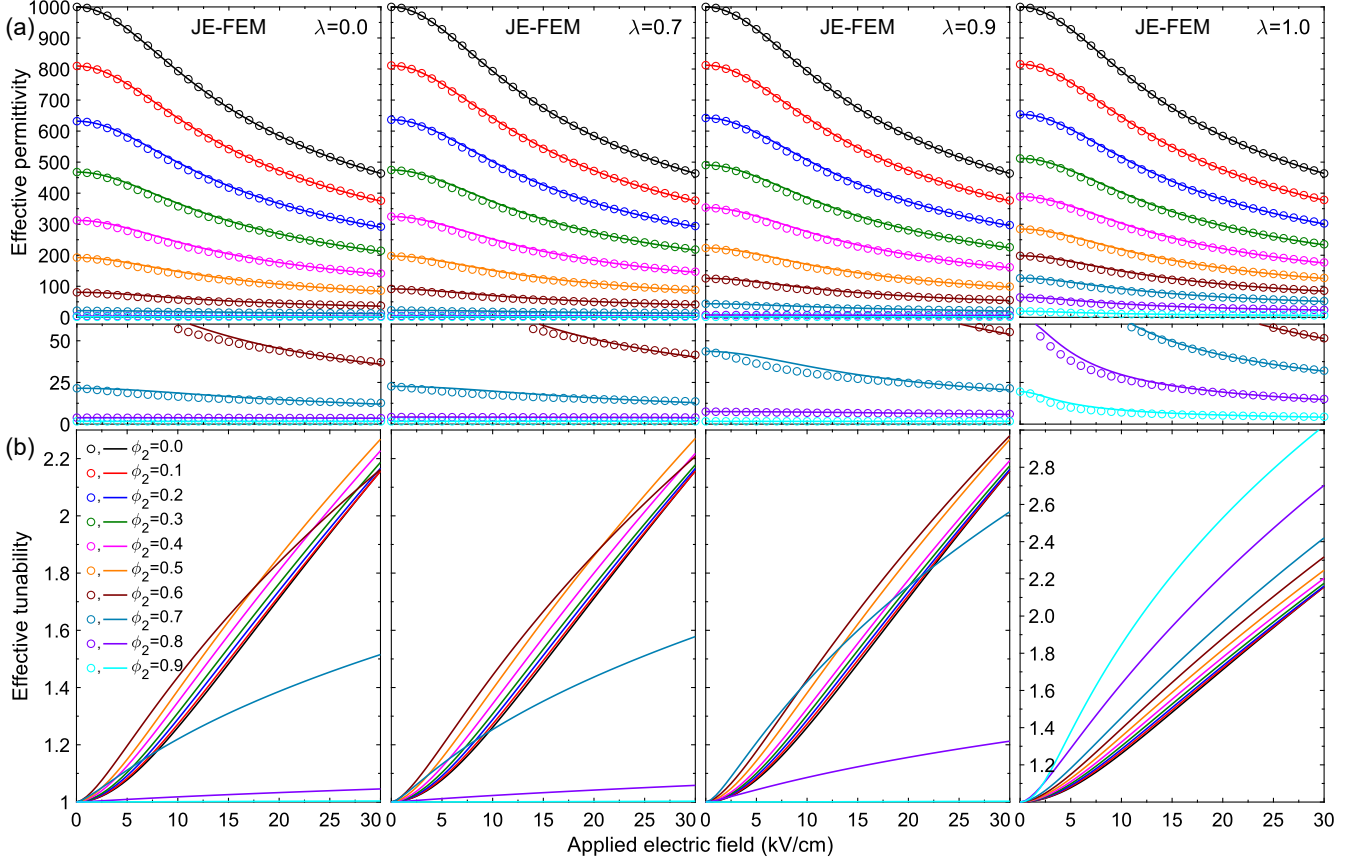


Figure 5: Effective permittivity (a, dots) and tunability (b, curves) of the random composite as a function of the applied electric field calculated by using JE-FEM model for different values of the linear dielectric phase (disks) surface fraction  $\phi_2$  from 0 to 0.9 and the degree of impenetrability  $\lambda = 0, 0.7, 0.9, 1$ . Continuous curves in (a) correspond to fitting the calculated field-dependent effective permittivity (dots) with Johnson's Eq. 6 using the determined effective Landau coefficient  $\beta_{eff}$  shown in Figure 6(b).

285 high fields, while the LD-FEM tunability tends to converge at higher fields. Remarkably, for all percolating systems below their percolation thresholds ( $\phi_2 \lesssim \phi_{2c}$ ) our results for the JE-FEM and LD-FEM models demonstrate the high tunability values in the narrow range of  $n = 2.15 - 2.28$  and  $n = 3.56 - 3.67$  at 30 kV/cm, respectively, with the maximum tunability attained for the disk surface fractions in the range 0.5 – 0.6 depending on  $\lambda$ . However, much  
 290 higher tunability than for a bulk paraelectric is reached for the non-percolating systems ( $\lambda = 1$ ) with disk surface fractions above  $\phi_2 \gtrsim 0.5$ . Specifically, at  $\phi_2 = 0.9$  corresponding to a periodic hexagonal array of disks in a matrix, the tunability reaches its maximum value of

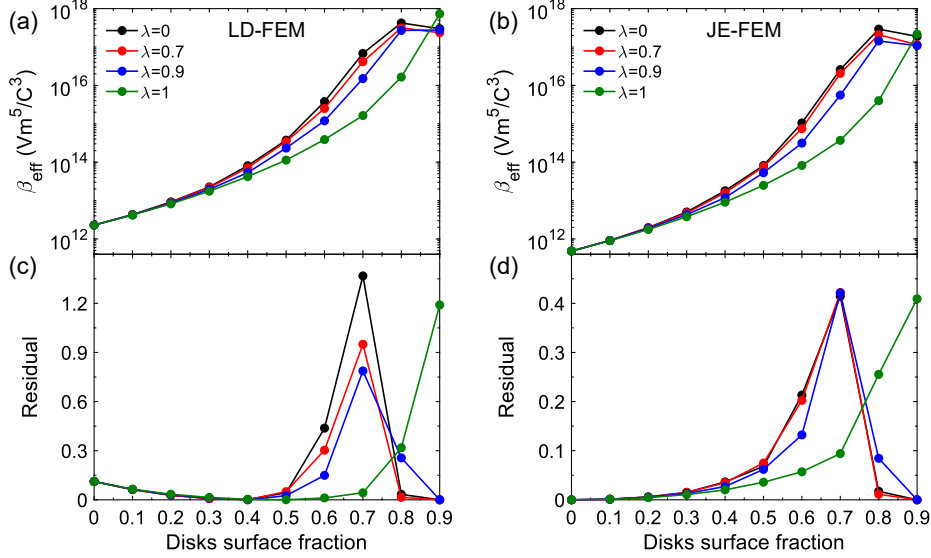


Figure 6: (a,b) Effective Landau coefficient  $\beta_{eff}$  determined by fitting the calculated LD-FEM (a) and JE-FEM (b) field-dependent effective permittivities shown respectively in Figures 3(a) and 5(a) (dots) with Johnson's Eq. 6. (c,d) Residual determined as a sum of the squares of the relative difference between the calculated LD-FEM (c) and JE-FEM (d) effective permittivities and the respectively fitted with Johnson's Eq. 6 effective permittivities using coefficients  $\beta_{eff}$  in (a) and (b). The calculated LD-FEM and JE-FEM effective permittivities (dots) together with their fitted counterparts (curves) are shown in Figures 3(a) and 5(a), respectively. The data were calculated for different values of the linear dielectric phase (disks) surface fraction  $\phi_2$  from 0 to 0.9 and the degree of impenetrability  $\lambda = 0, 0.7, 0.9, 1$ .

$\sim 3.02$  and  $\sim 4.44$  at  $30 \text{ kV/cm}$  for the JE-FEM and LD-FEM models, respectively. Though, the increased porosity in this case may raise questions about the mechanical stability and electrical reliability (breakdown) of these materials.

295

So far we have presented the complex numerical simulations with explicit account of full microstructure information of the continuum disordered systems leading to a highly inhomogeneous local fields which in turn govern the tunability properties. In what follows, we demonstrate that by appropriate modification of the Landau coefficient of nonlinearity  $\beta$  in the semi-empirical Johnson's equation (Eq. 6) permits us to accurately describe the effective permittivity of a wide variety of models of our paraelectric-dielectric composite medium. For that, we have determined the effective nonlinearity parameter  $\beta_{eff}$  by linear regression analysis fitting the LD-FEM (Figure 3(a), dots) and JE-FEM (Figure 5(a), dots) field-dependent effective permittivities with the Johnson's Eq. 6. The dependence of the effective parameter

300

$\beta_{eff}$  over the entire range of concentration of the linear dielectric phase and the degree of impenetrability considered is shown in Figure 6(a) and (b) for the LD-FEM and JE-FEM models, respectively. A similar trend for both models is observed. First of all, it is apparent that  $\beta_{eff}$  values significantly differ from the  $\beta$  parameter of the bulk paraelectric phase used as the input in the numerical calculations. The  $\beta_{eff}$  for all impenetrability parameters  $\lambda$  continuously and strongly increases with the concentration of the dielectric disk phase with the observation that the larger the  $\lambda$  the smaller the  $\beta_{eff}$ . For instance,  $\beta_{eff}$  increases in the range from  $4.82 \cdot 10^{11} / 2.30 \cdot 10^{12} \text{ V} \cdot \text{m}^5 / \text{C}^3$  ( $\phi_2 = 0$ ) to  $2.92 \cdot 10^{17} / 7.30 \cdot 10^{17} \text{ V} \cdot \text{m}^5 / \text{C}^3$  ( $\phi_2 = 0.9$ ) for the JE/LD-FEM models. This increase can be attributed mainly to the appearance of inhomogeneous local electric field fluctuations caused by increased interfacial contact area between the paraelectric and dielectric phases, degrees of disk aggregation present in the system, and consequently, enhanced multipolar interactions. In this regard, our results for the  $\beta_{eff}$  trend are in close agreement with those obtained in previous experimental [48, 49] and simulation [30] studies on other composites. It is important to note about discrepancy between the fitted values of  $\beta_{eff}$  for the bulk paraelectric phase ( $\phi_2 = 0$ ) in the JE-FEM and LD-FEM models. While this value for the former model coincides with  $\beta$  parameter used as the input in numerical calculations, i.e.  $\beta_{eff} = \beta = 4.82 \cdot 10^{11} \text{ V} \cdot \text{m}^5 / \text{C}^3$ , the value of  $\beta_{eff}$  for the latter is more than four times higher than the  $\beta$ , i.e.  $\beta_{eff} = 2.30 \cdot 10^{12} \text{ V} \cdot \text{m}^5 / \text{C}^3$ . This is due to the fact that the Johnson's equation is only valid for small applied fields and small polarization, and therefore, cannot describe exactly the LD-FEM results calculated for a large range of the applied fields by taking into account the higher order polarization terms.

The fitted solid curves in Figures 3(a) and 5(a) demonstrate that the Johnson's equation fits quite well, respectively, the LD-FEM and JE-FEM numerical data (dots) over the entire range of disk surface fraction and the degree of impenetrability considered, though some considerable deviations are observed to a greater extent for the former. To measure and compare the accuracy of the fits for both models, we also plot in Figure 6(c),(d) a computed residual for each system defined as a sum of the squares of the relative difference between the numerical LD/JE-FEM effective permittivities ( $\varepsilon_{FEM}$ ) and the fitted with Johnson's dependency ( $\varepsilon_{Johnson}$ )

$$R = \sum ((\varepsilon_{FEM} - \varepsilon_{Johnson}) / \varepsilon_{FEM})^2. \quad (13)$$

In other words, the lower the residual the better the Johnson's equation fits the numerical data. A few comments are in order here. First of all, our data suggest that the the Johnson's equation does not fit the simulation data equally well over the entire range of surface fraction and whatever is the degree of impenetrability considered. Second, a comparison of the residuals for both models shows that overall the Johnson's equation describes more accurately the JE-FEM data than the LD-FEM data, as intuitively expected. Third, as already pointed out in the previous paragraph, while the Johnson's equation describes exactly the JE-FEM data for the pure paraelectric material, i.e. the residual  $R_{JE-FEM}(\phi_2 = 0) = 0$ , it fails to represent well the LD-FEM data for the pure paraelectric manifested in the non-zero value of the residual  $R_{LD-FEM}(\phi_2 = 0) = 0.11$ . Next, what is noticeable in Figure 6(c),(d) is that, the residual for the two models follows a different trend for disk surface fractions  $\phi_2 \lesssim 0.5$  and the same trend for  $\phi_2 \gtrsim 0.5$ . For the JE-FEM model, the zero value residual at  $\phi_2 = 0$  increases slowly with increasing the concentration of the linear dielectric phase up to  $\phi_2 \approx 0.5$ , while for the LD-FEM model the non-zero value of the residual at  $\phi_2 = 0$  decreases slowly. Thus, the Johnson's equation describes more accurately the LD-FEM data for values of  $\phi_2$  in the range  $0.3 \leq \phi_2 \leq 0.5$ . Then, Figure 6(c),(d) reveals that the global features of the residual above  $\phi_2 \gtrsim 0.5$  are different for the percolative and nonpercolative systems, indicating that particle connectivity has a great impact on the accuracy of the fit. For the percolating systems in both models, the residual increases abruptly up to  $\phi_2 \approx 0.7$ , and then sharply decreases for  $\phi_2 \gtrsim 0.7$ . This abrupt variation of the residual is clear suggestion of a critical transition associated with percolation threshold which emerges in these composites at the surface fractions in the range  $0.69 \leq \phi_{2c} \leq 0.76$  depending on  $\lambda$ . Indeed, the paraelectric matrix discontinuity and associated large electric field enhancement near the percolation threshold lead to abnormal behaviour of the field-dependent effective permittivity, reflected in high nonlinearity of the tunability as can be seen in Figures 3(b) and 5(b), and thus the worse accuracy of the fit. For the higher surface fractions of linear dielectric phase,  $\phi_2 \geq 0.8$ , the strong linearization of the field-dependent effective permittivity explains the significant reduction of the residual. On the other hand, for the nonpercolating systems in both models, the residual increases continuously with  $\phi_2$ . Overall, Figure 6 demonstrates that the semi-empirical Johnson's equation with only one fitting parameter can be used to describe the

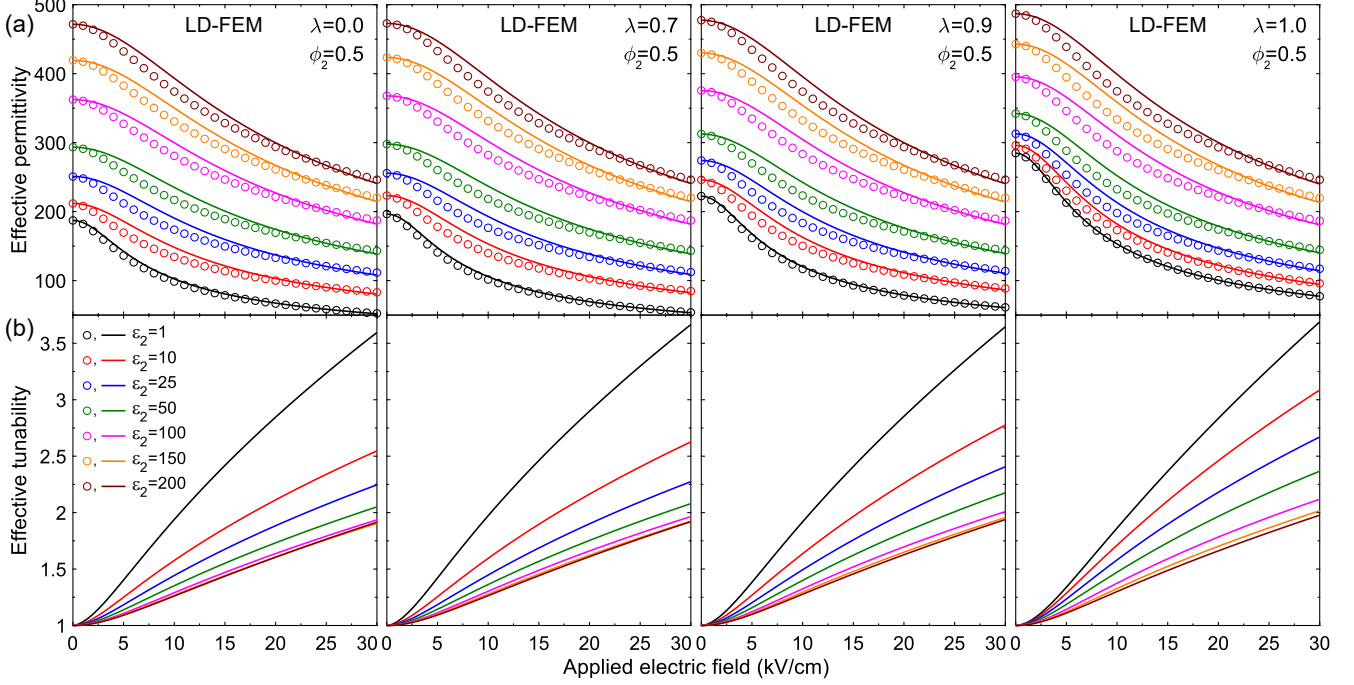


Figure 7: Effective permittivity (a, dots) and tunability (b, curves) of the random composite as a function of the applied electric field calculated by using LD-FEM model for different values of the linear dielectric phase (disks) permittivity  $\varepsilon_2$  from 1 to 200. The data were calculated for the surface fraction of disks  $\phi_2 = 0.5$  and degree of impenetrability  $\lambda = 0, 0.7, 0.9, 1$ . Continuous curves in (a) correspond to fitting the calculated field-dependent effective permittivity (dots) with Johnson’s Eq. 6 using the determined effective Landau coefficient  $\beta_{eff}$  shown in Figure 8(a).

field-dependent effective permittivity with a certain accuracy and establishes a link between the Johnson’s equation and LD theory which have been used to describe the tunability of paraelectric composites.

In the physical systems like those described above, generically the nonlinear dielectric behaviour depends not only on the microstructure characteristics but also on the properties of their constituents. So far we have presented our simulations for the systems consisting of disks of relative permittivity  $\varepsilon_2 = 1$  randomly distributed throughout the paraelectric matrix, i.e. for the porous paraelectrics. Next, we investigate the role of the linear dielectric phase permittivity on the effective permittivity and tunability of the composite by employing LD-FEM model and varying the relative permittivity of disks in the range  $1 \leq \varepsilon_2 \leq 200$ . Our results for the surface fraction  $\phi_2 = 0.5$  (i.e. all systems are well below their percolation

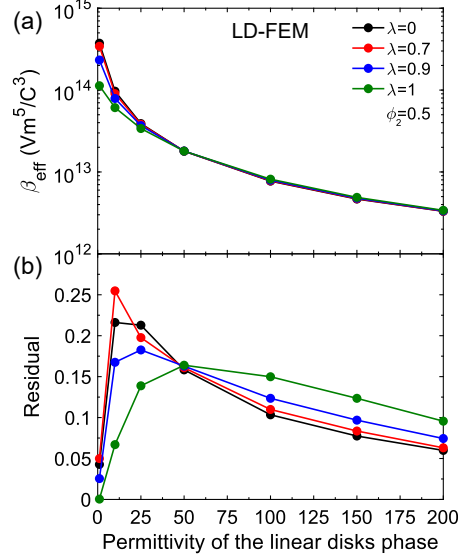


Figure 8: (a) Effective Landau coefficient  $\beta_{eff}$  determined by fitting the calculated LD-FEM field-dependent effective permittivity shown in Figures 7(a) (dots) with Johnson’s Eq. 6. (b) Residual determined as a sum of the squares of the relative difference between the calculated LD-FEM effective permittivities (Figures 7(a), dots) and the fitted with Johnson’s Eq. 6 effective permittivities (Figures 7(a), curves) using the coefficients  $\beta_{eff}$  in (a). The data were calculated for the fixed surface fraction of disks  $\phi_2 = 0.5$  and different values of the linear dielectric phase (disks) permittivity  $\epsilon_2$  from 1 to 200 and the degree of impenetrability  $\lambda = 0, 0.7, 0.9, 1$ .

thresholds for all  $\lambda$ ) and different values of  $\lambda$  and  $\epsilon_2$  are displayed compactly in Figure 7. For all values of  $\lambda$ , the dependencies of  $\epsilon_{eff}$  (Figure 7(a), dots) and tunability (Figure 7(b), curves) on  $E_{app}$  reveal the same systematic trend in the progressive increase of the zero-  
 370 field effective permittivity and continuous decrease of the tunability with the increase of  $\epsilon_2$ . Furthermore, for a given value of  $\epsilon_2$ , both  $\epsilon_{eff}$  and tunability increase as a function of the impenetrability parameter  $\lambda$ . More specifically, the highest tunability is observed for the porous paraelectric composite ( $\epsilon_2 = 1$ ) due to the highest phases permittivity contrast and consequently strongest polarization of the medium leading to the most intense spatial  
 375 distribution of the electric field. It is also important to note that the tunability decreases more rapidly for the smaller values of  $\epsilon_2$ , and thus, only for  $\epsilon_2$  close to 1 the tunability values are comparable to the those of the single-phase paraelectric for all range of  $\lambda$  (see Figure 3(b), black curves). Nevertheless, these numerical results offer possibilities for tailoring dielectric and tunability properties in a certain range through a properly chosen filler material. They  
 380 also highlight the crucial sensitivity of the tunability properties to the permittivity contrast

between the phases in this composite.

By fitting the LD-FEM permittivity data (dots) with the Johnson's equation (Eq. 6), we determined the effective nonlinearity parameter  $\beta_{eff}$  and then calculated the corresponding residual over the entire range of  $\varepsilon_2$  and  $\lambda$  as plotted in Figure 8. As expected, the  $\beta_{eff}$  parameter for all  $\lambda$  decreases monotonically as  $\varepsilon_2$  is increased towards the zero-field permittivity of the nonlinear phase ( $\varepsilon_1(0) = 1000$ ), and eventually would approach the value of the bulk paraelectric material for  $\varepsilon_2 = 1000$ , i.e.  $\beta_{eff} = 2.30 \cdot 10^{12} \text{ V} \cdot \text{m}^5 / \text{C}^3$ . Another observation is that the variance of  $\beta_{eff}$  as a function of  $\lambda$  at a given  $\varepsilon_2$  is decreased as  $\varepsilon_2$  is increased. Interestingly, the dependence of the residual on  $\varepsilon_2$  (Figure 8(b)) shows the varying trend, but the smallest residual and thus the best fit is observed for the porous paraelectric (see Figure 7(a), black curves).

We further examine the effect of the Landau coefficient of dielectric nonlinearity  $\beta$  (see LD Eq. 10) of the paraelectric matrix in these systems by varying  $\beta$  between  $1 \cdot 10^{11}$  and  $9 \cdot 10^{11} \text{ V} \cdot \text{m}^5 / \text{C}^3$  and fixing the surface fraction at  $\phi_2 = 0.5$ . The LD-FEM data presented in Figure 9 demonstrates the trend of the progressive increase in the nonlinearity of the field-dependent effective permittivity and in turn the tunability with the increase in  $\beta$ . Likewise, this figure nicely illustrates the effect of the degree of disk impenetrability  $\lambda$  on the effective permittivity of the resulting microstructures. Interestingly, while for a given  $\beta$  the effective zero-field permittivity remarkably increases as a function of  $\lambda$ , the tunability increases slightly. In addition to these features, we also note that the Johnson's equation fittings for all configurations (Figure 9a, curves) describe the LD-FEM numerical data (Figure 9a, dots) with an excellent accuracy. In this regards, one can observe two tendencies in Figure 10: (a) the larger the coefficient of the nonlinearity  $\beta$  the larger  $\beta_{eff}$  and residual; (b) for a given  $\beta$  the larger the  $\lambda$  the smaller the  $\beta_{eff}$  and residual, showing a considerable impact of the connectedness and clustering of disks on the  $\beta_{eff}$  and accuracy of the fits.

So far, we have focused on composites consisting of the dielectric disks randomly distributed in the paraelectric matrix. In what follow, we aim to investigate the impact of the periodicity in 2D composite systems on the tunability properties. Figure 11 compares the effective permittivity and tunability of the three different composite configurations, namely consisting of the random, periodic square and hexagonal arrays of dielectric impenetrable

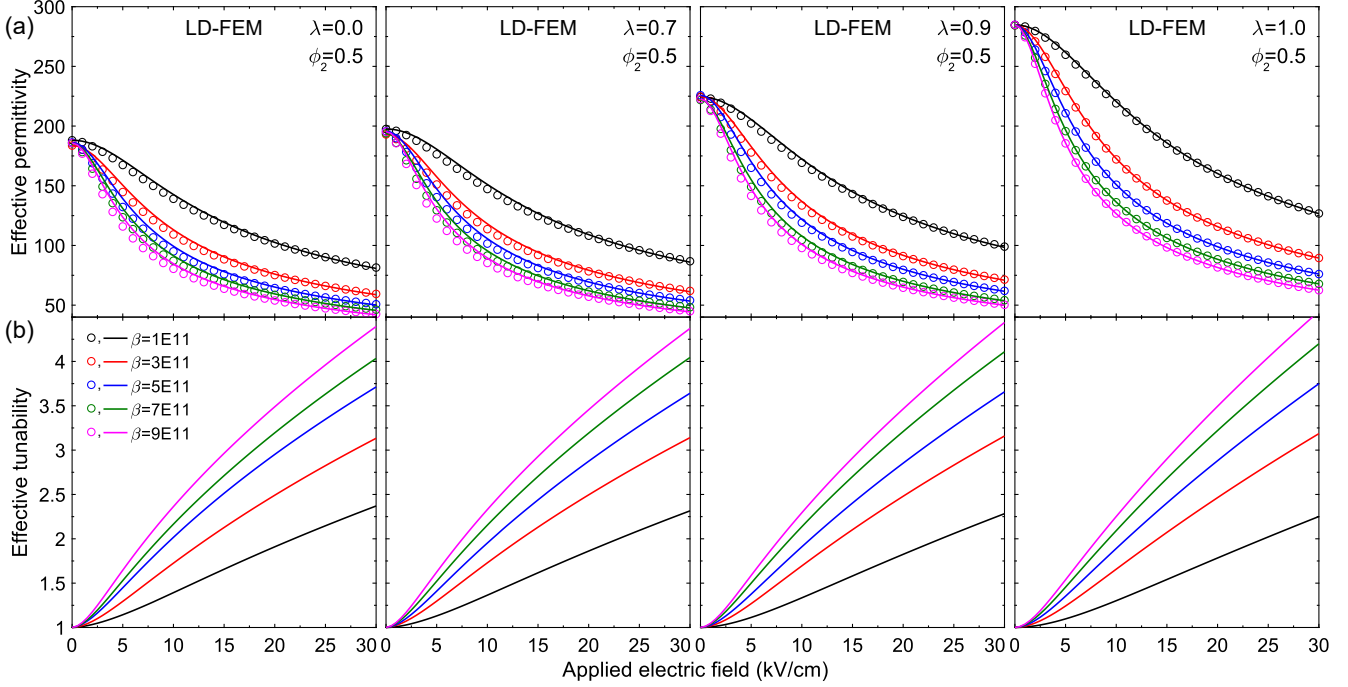


Figure 9: Effective permittivity (a, dots) and tunability (b, curves) of the random composite as a function of the applied electric field calculated by using LD-FEM model for different values of the nonlinear Landau coefficient of the paraelectric matrix  $\beta$  from  $1 \cdot 10^{11}$  to  $9 \cdot 10^{11} \text{ V}\cdot\text{m}^5/\text{C}^3$ . The data were calculated for the surface fraction of disks  $\phi_2 = 0.5$  and degree of impenetrability  $\lambda = 0, 0.7, 0.9, 1$ . Continuous curves in (a) correspond to fitting the calculated field-dependent effective permittivity (dots) with Johnson’s Eq. 6 using the determined effective Landau coefficient  $\beta_{eff}$  shown in Figure 10(a).

disks ( $\lambda = 1$ ) in the paraelectric matrix. It is worthy to note that the maximum close packing fraction of hard disks for the square, random, and hexagonal arrays is known to be  $\phi_2^{max} \cong 0.785, 0.86,$  and  $0.907,$  respectively, so we are limited by these values of disk surface fraction for each particular array. It is quite remarkable that the effective permittivity for all three arrays (Figure 11(a)) demonstrates a distinct behaviour. Namely, the value of the zero-field effective permittivity of the random array (dots) for a particular surface fraction is smaller than that of the square array (solid curves), which in turn is smaller than that of the hexagonal array (dashed curves). Furthermore, the difference between these values increases monotonically as the disk surface fraction is increased. Importantly, this plot also clearly reveals that the periodic square array possesses the strongest nonlinear response of the field-dependent effective permittivity, i.e. the strongest field-dependent effective permit-

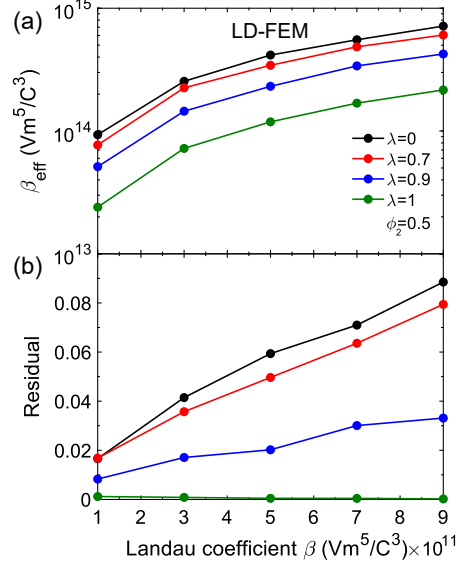


Figure 10: (a) Effective Landau coefficient  $\beta_{eff}$  determined by fitting the calculated LD-FEM field-dependent effective permittivity shown in Figures 9(a) (dots) with Johnson’s Eq. 6. (b) Residual determined as a sum of the squares of the relative difference between the calculated LD-FEM effective permittivities (Figures 9(a), dots) and the fitted with Johnson’s Eq. 6 effective permittivities (Figures 9(a), curves) using the coefficients  $\beta_{eff}$  in (a). The data were calculated for the fixed disk surface fraction  $\phi_2 = 0.5$ , different values of the Landau coefficient of paraelectric matrix  $\beta$  from  $1 \cdot 10^{11}$  to  $9 \cdot 10^{11} \text{ V}\cdot\text{m}^5/\text{C}^3$  and the degree of impenetrability  $\lambda = 0, 0.7, 0.9, 1$ .

tivity variation as compared to others. Indeed, the largest tunability among the three arrays is achieved for the periodic square array (Figure 11(b)), while the intermediate and smallest ones for the random (Figure 11(c)) and hexagonal (Figure 11(d)) arrays, respectively. As  
425 expected, all composites exhibit a continuous growth of the tunability with the disk surface fraction, though the magnitude of this growth is different in each case. Again, the fastest growing tunability is observed for the square array, while for the random array this growth is a bit smaller. In contrast, for the hexagonal array, the tunability increases insignificantly in a wide range of surface fractions  $0 \leq \phi_2 \leq 0.7$ . Actually, there is a simple explanation for  
430 the distinct grow and magnitude of the tunability in these arrays. The simple square and hexagonal arrays ensure respectively the closest and the farthest particle-particle distance in the composite for the same  $\phi_2$ . As shown above, the closer contact between neighboring inclusions produces the stronger electric field enhancement confined in a paraelectric matrix between inclusions, which actually explains the large tunability values for the square

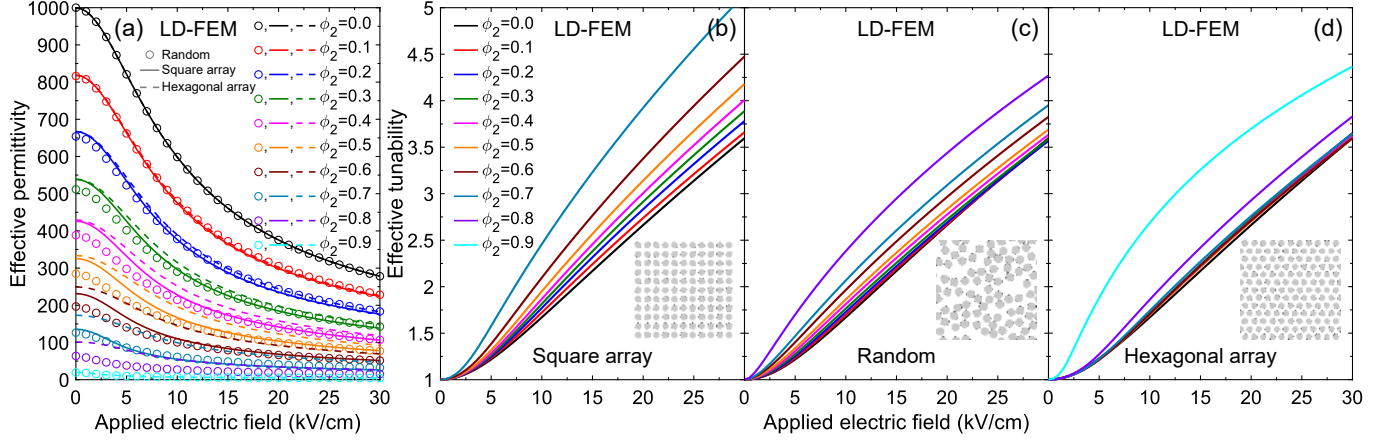


Figure 11: (a) Effective permittivity of the random (dots), periodic square (solid curves) and hexagonal (dashed curves) arrays of dielectric impenetrable disks in a paraelectric matrix as a function of the applied electric field calculated by using LD-FEM model for different values of the disk surface fraction  $\phi_2$  and degree of impenetrability  $\lambda = 1$ . (b-d) Same as in (a) for effective tunability (solid curves) of the periodic square (b), random (c), and periodic hexagonal (d) arrays of dielectric impenetrable disks in a paraelectric matrix.

array. Obviously, the values of tunability of the random disk configurations must be in  
between those two extreme cases. Furthermore, the tiny increase of tunability for surface  
fractions  $\phi_2 \leq 0.7$  in the hexagonal array is because the particles start to significantly “feel”  
each other for larger values of surface fractions, i.e., when the distance between particles  
becomes smaller. Nevertheless, this peculiar feature of the periodic hexagonal array can  
be useful for certain applications where different field-dependent effective permittivities and  
same tunabilities are required.

## 5. Conclusions

In this work we have numerically investigated nonlinear dielectric properties of the 2D  
random paraelectric-dielectric composite consisting of monodisperse disks with an arbitrary  
degree of impenetrability of a dielectric phase randomly dispersed in the continuous matrix  
of the paraelectric phase. Our simulations reveal that the geometrical percolation threshold  
in this composite governs the critical behavior of the effective permittivity and tunability.  
Below the percolation threshold, our simulations show a strong nonlinear behavior of the  
field-dependent permittivity and high tunability that increases as a function of dielectric

450 phase concentration. Above the percolation threshold, the permittivity shows the tendency to linearization and the tunability dramatically drops down. Actually, the presence of percolation transition explains why many experimental works demonstrate the drop of tunability at the intermediate values of concentration of the linear dielectric phase. In contrast, for the nonpercolating structures with prohibited disk overlaps the tunability increases with the  
 455 concentration of the dielectric phase up to the highest possible concentrations. Therefore, the large values of tunability and highly reduced permittivity are possible at the arbitrarily large values of the linear dielectric phase concentration if we avoid triggering the percolation transition within the system. Indeed, our simulations demonstrate the extraordinarily high tunability obtained for the random composite with impenetrable dielectric disks at high con-  
 460 centrations. Furthermore, even higher tunability is revealed in the 2D periodic square array of dielectric disks in the paraelectric matrix. Notably, our study also shows that only the porous paraelectrics and paraelectrics filled with materials of very low dielectric constant possess the tunability which is comparable to that of the bulk paraelectric.

We are now ready to answer on an important open question which arises as to why  
 465 among various types of 2D random paraelectric-dielectric composites the reported tunability demonstrates the abrupt break down to the almost zero value above some critical concentration of the a linear dielectric phase, while for many 3D systems the tunability decreases more smoothly up to the high volume fractions of dielectric phase [50]. We believe that the explanation for this emerges from an apparent difference between 2D and 3D stochastic  
 470 heterogeneous systems. In the 2D systems the bicontinuous structure cannot exist, i.e., when the inclusion phase is sample-spanning (percolating), the matrix is discontinuous, while the 3D systems can be bicontinuous that actually allows the high electric field to be concentrated in both the paraelectric and dielectric phases, in contrast to the 2D systems. For instance, it was demonstrated that for a 3D composite consisting of fully-penetrable spheres  
 475 randomly placed in a matrix both the inclusion phase and the matrix are sample spanning for  $0.29 \leq \phi_2 \leq 0.97$  [51]. Furthermore, the percolation threshold for spheres with different degree of impenetrability ( $\phi_{2c} \geq 0.29$ ) is considerably lower than that for disks of equal diameters in 2D ( $\phi_{2c} \geq 0.67$ ). All of these imply the rather smooth decrease of tunability in such 3D composite starting already for volume fractions of dielectric spheres below  $\phi_{2c}$

480 (i.e. much lower than in the corresponding 2D composite) and ensure the nonzero value of tunability up to  $\phi_2 \approx 0.97$ .

The second contribution from the current work consists of a quantitative test of the semi-empirical Johnson's equation to describe the paraelectric-dielectric composites. Our simulations demonstrate that the proper modification of the Landau coefficient of nonlin-  
485 earity in the Johnson's equation permits us to use it macroscopically for the prediction of the effective permittivity of these systems with a certain accuracy covering wide ranges of structural and material parameters.

Finally, our work reveals a complex interplay between the structural parameters (pe-  
riodicity, randomness, phase concentration, degree of phases connectivity, and clustering  
490 characteristics) and induced local electric field inhomogeneity, which governs the overall behavior of the tunability properties. In particular, we show that disk impenetrability parameter provides an additional degree of freedom in the manipulation of dielectric response of composites, which permits tailoring different combinations of the reduced permittivity and tunability. Overall, this detailed numerical study unveils a critical role of the microstructure  
495 and casts light on the tunability properties of the disordered percolating and nonpercolating composite media. We hope that our work will stimulate experimental efforts along this line because this simple composite model apart from possessing the enhanced tunability allows us to tailor nonlinear dielectric properties over a wide range of structural parameters through the manipulation with microstructures.

## 500 **Acknowledgements**

V.M. and J.F. acknowledge computing time at PC<sup>2</sup> Paderborn Center for Parallel Computing. This research did not receive any specific grant from funding agencies in the public, commercial, or not-for-profit sectors.

## **References**

- 505 [1] M. E. Lines, A. M. Glass, Principles and applications of ferroelectrics and related materials, International series of monographs on physics, Clarendon Press, 1977.

- [2] S. Gevorgian, *Ferroelectrics in Microwave Devices, Circuits and Systems: Physics, Modeling, Fabrication and Measurements*, Engineering Materials and Processes, Springer-Verlag London, 2009.
- 510 [3] O. G. Vendik, E. K. Hollmann, A. B. Kozyrev, A. M. Prudan, Ferroelectric tuning of planar and bulk microwave devices, *Journal of Superconductivity* 12 (1999) 325–338.
- [4] A. K. Tagantsev, V. O. Sherman, K. F. Astafiev, J. Venkatesh, N. Setter, Ferroelectric materials for microwave tunable applications, *J. Electroceram.* 11 (1–2) (2003) 5–66.
- 515 [5] P. Bao, T. J. Jackson, X. Wang, M. J. Lancaster, Barium strontium titanate thin film varactors for room-temperature microwave device applications, *Journal of Physics D: Applied Physics* 41 (6) (2008) 063001.
- [6] J. Im, O. Auciello, P. K. Baumann, S. K. Streiffer, D. Y. Kaufman, A. R. Krauss, Composition-control of magnetron-sputter-deposited  $(\text{Ba}_x)\text{Ti}_{1+y}\text{O}_{3+z}$  thin films for voltage tunable devices, *Applied Physics Letters* 76 (5) (2000) 625–627.
- 520 [7] G. Subramanyam, M. W. Cole, N. X. Sun, T. S. Kalkur, N. M. Sbrockey, G. S. Tompa, X. Guo, C. Chen, S. P. Alpay, G. A. Rossetti, K. Dayal, L.-Q. Chen, D. G. Schlom, Challenges and opportunities for multi-functional oxide thin films for voltage tunable radio frequency/microwave components, *Journal of Applied Physics* 114 (19) (2013) 191301.
- 525 [8] G. Shirane, K. Suzuki, On the phase transition in barium-lead titanate (i), *Journal of the Physical Society of Japan* 6 (4) (1951) 274–278.
- [9] C. L. Canedy, H. Li, S. P. Alpay, L. Salamanca-Riba, A. L. Roytburd, R. Ramesh, Dielectric properties in heteroepitaxial  $\text{Ba}_{0.6}\text{Sr}_{0.4}\text{TiO}_3$  thin films: Effect of internal stresses and dislocation-type defects, *Applied Physics Letters* 77 (11) (2000) 1695–1697.
- 530 [10] S.-J. Lee, S. E. Moon, H.-C. Ryu, M.-H. Kwak, Y.-T. Kim, S.-K. Han, Microwave properties of compositionally graded  $(\text{Ba},\text{Sr})\text{TiO}_3$  thin films according to the direction of the composition gradient for tunable microwave applications, *Applied Physics Letters* 82 (13) (2003) 2133–2135.

- [11] Q. Zhang, J. Zhai, L. B. Kong, Relaxor ferroelectric materials for microwave tunable applications, *Journal of Advanced Dielectrics* 02 (01) (2012) 1230002.
- [12] M. W. Cole, P. C. Joshi, M. H. Ervin, La doped  $\text{Ba}_{1-x}\text{Sr}_x\text{TiO}_3$  thin films for tunable device applications, *Journal of Applied Physics* 89 (11) (2001) 6336–6340.
- [13] U.-C. Chung, C. Elissalde, M. Maglione, C. Estournè, M. Paté, J. P. Ganne, Low-losses, highly tunable  $\text{Ba}_{0.6}\text{Sr}_{0.4}\text{TiO}_3/\text{MgO}$  composite, *Applied Physics Letters* 92 (4) (2008) 042902.
- [14] Y. He, Y. Xu, T. Liu, C. Zeng, W. Chen, Tunable dielectric properties of  $\text{BaZr}_{0.2}\text{Ti}_{0.8}\text{O}_3\text{-Mg}_2\text{SiO}_4\text{-MgO}$  composite ceramics, *Journal of Alloys and Compounds* 509 (3) (2011) 904–908.
- [15] J. Zhang, B. Shen, J. Zhai, X. Yao, In situ synthesis of  $\text{Ba}_{0.5}\text{Sr}_{0.5}\text{TiO}_3\text{-Mg}_2\text{TiO}_4$  composite ceramics and their effective dielectric response, *Scripta Materialia* 69 (3) (2013) 258–261.
- [16] X. Chou, J. Wang, Z. Zhao, W. Geng, W. Zhang, J. Zhai, Dielectric tunability and microwave properties of  $\text{Ba}_{0.5}\text{Sr}_{0.5}\text{TiO}_3\text{-BaMg}_6\text{Ti}_6\text{O}_{19}$  composite ceramics for tunable microwave device applications, *Journal of Electroceramics* 26 (1–4) (2011) 185.
- [17] L. Tang, J. Wang, J. Zhai, L. Bing Kong, X. Yao, Controllable-permittivity and high-tunability of  $\text{Ba}_{0.5}\text{Sr}_{0.5}\text{TiO}_3/\text{MgO}$  based ceramics by composite configuration, *Applied Physics Letters* 102 (14) (2013) 142907.
- [18] G. W. Milton, *The Theory of Composites*, Cambridge Monographs on Applied and Computational Mathematics, Cambridge University Press, 2002.
- [19] Y. Zhang, G. Wang, T. Zeng, R. Liang, X. Dong, Electric field-dependent dielectric properties and high tunability of porous  $\text{Ba}_{0.5}\text{Sr}_{0.5}\text{TiO}_3$  ceramics, *Journal of the American Ceramic Society* 90 (4) (2007) 1327–1330.
- [20] W. Liao, R. Liang, G. Wang, F. Cao, X. Dong, Dielectric and tunable properties of bulk columnar  $\text{Ba}_{0.6}\text{Sr}_{0.4}\text{TiO}_3/\text{MgO}$  composites, *Ceramics International* 39 (1) (2013) 891–895.

- [21] S. Torquato, *Random Heterogeneous Materials: Microstructure and Macroscopic Properties*, Interdisciplinary Applied Mathematics, Springer New York, 2002.
- [22] C. Brosseau, A. Beroual, Computational electromagnetics and the rational design of new dielectric heterostructures, *Progress in Materials Science* 48 (5) (2003) 373–456.
- 565 [23] C. Brosseau, Modelling and simulation of dielectric heterostructures: a physical survey from an historical perspective, *Journal of Physics D: Applied Physics* 39 (7) (2006) 1277–1294.
- [24] T. C. Choy, *Effective Medium Theory: Principles and Applications*, International series of monographs on physics, Clarendon Press, 1999.
- 570 [25] A. H. Sihvola, *Electromagnetic Mixing Formulas and Applications*, IEE electromagnetic waves series, Institution of Electrical Engineers, 1999.
- [26] K. F. Astafiev, V. O. Sherman, A. K. Tagantsev, N. Setter, Can the addition of a dielectric improve the figure of merit of a tunable material?, *Journal of the European Ceramic Society* 23 (14) (2003) 2381–2386.
- 575 [27] V. O. Sherman, A. K. Tagantsev, N. Setter, D. Iddles, T. Price, Ferroelectric-dielectric tunable composites, *Journal of Applied Physics* 99 (7) (2006) 074104.
- [28] K. Zhou, S. A. Boggs, R. Ramprasad, M. Aindow, C. Erkey, S. P. Alpay, Dielectric response and tunability of a dielectric-paraelectric composite, *Applied Physics Letters* 93 (10) (2008) 102908.
- 580 [29] L. Padurariu, L. Curecheriu, V. Buscaglia, L. Mitoseriu, Field-dependent permittivity in nanostructured BaTiO<sub>3</sub> ceramics: Modeling and experimental verification, *Phys. Rev. B* 85 (2012) 224111.
- [30] L. Padurariu, L. P. Curecheriu, L. Mitoseriu, Nonlinear dielectric properties of paraelectric-dielectric composites described by a 3D finite element method based on landau-devonshire theory, *Acta Materialia* 103 (2016) 724–734.
- 585

- [31] M. Lei, The impact of composite effect on dielectric constant and tunability in ferroelectric–dielectric system, *Journal of the American Ceramic Society* 98 (10) (2015) 3250–3258.
- [32] Y. Zhang, G. Wang, K. Wang, Y. Wang, X. Dong, The model of electric field dependent dielectric properties for porous ceramics, *Journal of Applied Physics* 103 (11) (2008) 114103.
- [33] L. Padurariu, L. Curecheriu, C. Galassi, L. Mitoseriu, Tailoring non-linear dielectric properties by local field engineering in anisotropic porous ferroelectric structures, *Applied Physics Letters* 100 (25) (2012) 252905.
- [34] R. E. Stanculescu, N. Horchidan, C. Galassi, M. Asandulesa, L. Padurariu, C. E. Ciomaga, L. Mitoseriu, Porous (Ba,Sr)TiO<sub>3</sub> ceramics for tailoring dielectric and tunability properties: Modelling and experiment, *Processing and Application of Ceramics* 11 (4) (2017) 235–246.
- [35] A. F. Devonshire, Theory of ferroelectrics, *Advances in Physics* 3 (10) (1954) 85–130.
- [36] C. Ang, Z. Yu, dc electric-field dependence of the dielectric constant in polar dielectrics: Multipolarization mechanism model, *Phys. Rev. B* 69 (2004) 174109.
- [37] K. M. Johnson, Variation of dielectric constant with voltage in ferroelectrics and its application to parametric devices, *Journal of Applied Physics* 33 (9) (1962) 2826–2831.
- [38] J. Zhang, J. Zhai, X. Chou, J. Shao, X. Lu, X. Yao, Microwave and infrared dielectric response of tunable Ba<sub>1-x</sub>Sr<sub>x</sub>TiO<sub>3</sub> ceramics, *Acta Materialia* 57 (15) (2009) 4491–4499.
- [39] Q. Xu, D. Zhan, H.-X. Liu, W. Chen, D.-P. Huang, F. Zhang, Evolution of dielectric properties in BaZr<sub>x</sub>Ti<sub>1-x</sub>O<sub>3</sub> ceramics: Effect of polar nano-regions, *Acta Materialia* 61 (12) (2013) 4481–4489.
- [40] D. P. Landau, K. Binder, *A Guide to Monte Carlo Simulations in Statistical Physics*, 4th Edition, Cambridge University Press, 2014.
- [41] M. Sahimi, *Applications Of Percolation Theory*, Taylor & Francis, 2003.

- [42] V. Myroshnychenko, C. Brosseau, Possible manifestation of nonuniversality in some continuum percolation systems, *Journal of Physics D: Applied Physics* 41 (9) (2008) 095401.
- 615 [43] V. Myroshnychenko, C. Brosseau, Effective complex permittivity of two-phase random composite media: A test of the two exponent phenomenological percolation equation, *Journal of Applied Physics* 103 (8) (2008) 084112.
- [44] V. Myroshnychenko, C. Brosseau, Effective complex permittivity and continuum percolation analysis of two-phase composite media, *IEEE Transactions on Dielectrics and*  
620 *Electrical Insulation* 16 (4) (2009) 1209–1222.
- [45] V. Myroshnychenko, C. Brosseau, Finite-element method for calculation of the effective permittivity of random inhomogeneous media, *Physical Review E* 71 (1) (2005) 016701.
- [46] E. Defay, T. Lacrovez, T. T. Vo, V. Sbrugnera, C. Bermond, M. Aïd, B. Fléchet, Ferroelectric properties of  $\text{Pb}(\text{Zr},\text{Ti})\text{O}_3$  thin films until 40 GHz, *Applied Physics Letters*  
625 94 (5) (2009) 052901.
- [47] Comsol multiphysics<sup>®</sup> v. 5.0., [www.comsol.com](http://www.comsol.com). COMSOL AB, Stockholm, Sweden (2014).
- [48] X.-F. Zhang, Q. Xu, D. Zhan, H.-X. Liu, W. Chen, D.-P. Huang, Dielectric response of MgO-added  $\text{Ba}_{0.6}\text{Sr}_{0.4}\text{TiO}_3$  ceramics under bias electric field: Examination of contributing mechanisms, *Physica B: Condensed Matter* 410 (2013) 170–176.  
630
- [49] P. Ren, H. Fan, X. Wang, X. Tan, Modified tunable dielectric properties by addition of MgO on  $\text{BaZr}_{0.25}\text{Ti}_{0.75}\text{O}_3$  ceramics, *Materials Research Bulletin* 46 (12) (2011) 2308–2311.
- [50] L. Padurariu, L. Mitoseriu, Comment on “The impact of composite effect on dielectric constant and tunability in ferroelectric-dielectric system”, *Journal of the American Ceramic Society* 99 (11) (2016) 3816–3817.  
635
- [51] M. Sahimi, *Heterogeneous Materials I: Linear Transport and Optical Properties, Interdisciplinary Applied Mathematics*, Springer New York, 2006.